J. Fluid Mech. (1996), vol. 320, pp. 185–210

Instability of a liquid jet subject to disturbances composed of two wavenumbers

By H. HUYNH, N. ASHGRIZ AND F. MASHAYEK

Department of Mechanical and Aerospace Engineering, State University of New York at Buffalo, Buffalo, NY 14260, USA

(Received 8 September 1994 and in revised form 19 March 1996)

The instability of viscous capillary jets subject to disturbances consisting of two superposed wavenumbers, and for large disturbance amplitudes is investigated. Disturbances composed of the superposition of a fundamental disturbance (first harmonic) with either its second or third harmonic are used. The influence of the wavenumber of the fundamental disturbance on the jet breakup is studied for a disturbance composed of a first harmonic with an initial non-dimensional amplitude of $\epsilon_1 = 0.01$ and a second harmonic with an initial non-dimensional amplitude of $\epsilon_2 = 0.05$. The influence of the initial amplitudes of the first and second harmonics on the jet breakup is studied for two non-dimensional wavenumbers of the fundamental (first harmonic): $k = 0.45$ and $k = 0.7$; the second harmonic is unstable in the former and stable in the latter case. The effect of an added third harmonic is studied only for $k = 0.45$ but for a wide range of initial amplitudes. All cases are studied for an in-phase and a 180° out-of-phase superposition of the two waves. The nonlinear interaction between the two waves results in the formation of a variety of drop sizes and shapes. The breakup times can be controlled within a wide range using this technique.

1. Introduction

The use of capillary instability of a liquid jet has been one of the most common techniques for the production of spherical drops with uniform sizes. When a liquid jet is subjected to a monochromatic (single-wavenumber) disturbance with a wavenumber less than the cut-off wavenumber, it becomes unstable and breaks up. Each wavelength of the input disturbance usually generates two types of drops: a large main drop and one or more smaller satellite drops. Generally, the size of the satellite drops reduces with increasing (decreasing) the wavenumber (wavelength) and decreasing the Reynolds number (see Ashgriz & Mashayek 1995, and references therein). (In the temporal instability analysis of liquid jets, the Reynolds number is defined based on the capillary wave speed. Therefore, it is the inverse of Ohnesorge number, $Re = 1/Oh = (1/\nu)(\gamma r_o/\rho)^{1/2}$, where ν is the kinematic viscosity, γ is the coefficient of the surface tension, ρ is the liquid density, and r_o is the jet radius.)

In order to obtain uniform-size drops, either the larger drops or the smaller drops are eliminated. This is achieved mainly by three different techniques: (i) preventing the initial formation of the satellite drops; (ii) forcing the satellite drops to merge with the main drops; (iii) charging and deflecting one of the drops. The experimental investigations of Bousfield, Stockel & Nanivadekar (1990) show that the formation of the satellite drops could be prevented only for jets with Reynolds numbers less than 0.44 (for their smallest wavenumber of $k = 0.26$). In addition, Ashgriz & Mashayek

(1995) provide a numerically determined boundary between the satellite/no-satellite regions in the Re,k space. They show that the no-satellite region is limited to small Reynolds numbers even for the wavenumbers close to the cut-off wavenumber. The satellite drops are persistently formed at Re larger than 4 for wavenumbers up to 0.95. The Reynolds number for many of the commonly used liquids is much larger than 4. For instance, a water jet with 1 mm diameter has a Reynolds number of 200. Therefore, other methods must be used to eliminate the satellite drop formation.

Satellite drops can also be eliminated by increasing the amplitude of the initial disturbance. This reduces the breakup time, and therefore, there is no time for the development of the satellite-forming liquid ligament. Ashgriz & Mashayek (1995) have shown that for a jet with $Re = 200$ the initial disturbance amplitude has to be as large as 80% of the jet radius in order to eliminate the satellites. Such high amplitudes, although possible, are impractical in most applications. In practice, however, the change in amplitude results in the forward or backward merging of satellite drops with the main drops and, therefore, the formation of uniform drops shortly after the breakup point. Satellite merging is due to the non-symmetric breakup of the liquid ligament. Pimbley & Lee (1977), Chaudhary & Maxworthy (1980*a*,*b*), Bousfield *et al.* (1990) and Vassallo & Ashgriz (1991) show experimentally that the forward or backward merging of the satellites with the main drops can occur at various applied disturbance frequencies depending on the amplitude of the disturbance.

A more practical method of eliminating the formation of the satellite drops is by using a modulated disturbance. Chaudhary & Maxworthy (1980*a*,*b*) and Scheller & Bousfield (1991) provide results of such experiments. They use a modulated velocity disturbance composed of two frequencies, and show that the satellite drop formation can be most effectively prevented by the superposition of the first and third harmonics for certain ratios of the initial amplitudes of the two harmonics. Modulated disturbances are also used to force the merging of the satellites with the main drops after their formation. Although forward and backward merging occurs even with monochromatic disturbances, the merging can be expedited by using modulated disturbances. Chaudhary & Maxworthy (1980*b*), and Scheller & Bousfield (1991) use the two-frequency disturbances and measure the distance it takes for the satellite drops to merge with the main drops. They show that the merging distance depends on the amplitude ratio of the two frequencies and the phase angle between them. In addition, Orme & Muntz (1990) study the droplet formation experimentally by perturbing the jet with an amplitude-modulated velocity disturbance. They show that the small droplets merge into a final configuration where the uniform drops are equally separated by one wavelength of the modulation frequency. Orme et al. (1993) further obtain sequences of repeating drop patterns by adding non-integer frequency ratios (the ratio of the high to the low frequency).

The techniques described above are designed to eliminate the satellite drops. However, in many applications the satellite drops are the ones which are desired. For instance, in the high-resolution ink jet printers, the main drops are eliminated and the smaller satellite drops are used in printing (Yamada 1978). This is achieved by first charging the drops and then deflecting them using a charged electrode. The deflection amount is different for drops with different sizes. Therefore, a drop catcher can be used to intercept the flight path of the drops that are to be eliminated. In order to effectively (e.g. instantaneously and with small signal voltage) charge the drops, the liquid must have good and stabilized electrical conductivity. This imposes limitations on the type of liquid used. Smaller satellite drops can be easily deflected even if a relatively low-conductance liquid is used.

Although it is experimentally shown that the satellite drop size can be controlled by using modulated disturbances, a complete theoretical analysis of this problem has not been reported. The only analytical study is given by Chaudhary & Redekopp (1980). They consider the instability of a liquid jet subject to an initial velocity disturbance consisting of a fundamental (first harmonic) and one higher harmonic. They use the method of straining of coordinates and apply a third-order nonlinear analysis to an infinitely long cylindrical column of inviscid fluid. The second- and third-order solutions show interactions between the fundamental and the harmonic, and feedbacks to the original inputs. Their third-order solution indicates that satellite drops form only for $k < 0.65$ and no satellite exists for $k > 0.65$. This is contrary to the experimental observations, exemplified by those of Vassallo & Ashgriz (1991), and the complete solution of the nonlinear equations by Ashgriz & Mashayek (1995) who show that for liquid columns with $Re > 4$, the satellite drops are persistently formed for the unstable wavenumbers, i.e. $k < 1$.

Another theoretical study in this area is given by Scheller & Bousfield (1991), who use the thin filament model of Bousfield *et al.* (1986). However, their main concern is to identify whether the liquid ligament will break up on the downstream or upstream side of the potential satellite drop, based on which backward or forward merging of the satellite drop can be predicted – no information on satellite size control is provided.

This paper follows the work of Ashgriz & Mashayek (1995) where satellite drop formation subject to a monochromatic perturbation is investigated. Our main concern in this paper is to control the breakup of a jet and the formation of the satellite drops by surface perturbation synthesis. We show that a variety of drop sizes and drop shapes can be obtained which may have important practical implications. The modulated disturbances have already been used to control satellite drop formation in ink jet printers. In addition, we discuss the 'breakup mechanism' of a liquid jet subject to large-amplitude two-wavenumber disturbances. (Recent advances in technology have provided means to obtain large-amplitude disturbances, e.g. see Dressler 1993.) We have simulated the instability of a viscous capillary jet, subject to an initial disturbance consisting of the superposition of the first harmonic with either the second or third harmonic. The problem and the numerical technique are described in §2. The breakup of the jet when the second harmonic is added to the initial disturbance and the effects of the wavenumber on the jet breakup are presented in §3. In §4, we consider the superposition of the first and third harmonics and describe the effects of the added harmonic amplitude. Concluding remarks are provided in §5.

2. Mathematical formulation

Two different approaches are possible when dealing with the problem of capillary jet instability. One is to investigate the spatial problem of a jet emanating from a nozzle, when the disturbance grows with distance along the jet. The other is to consider an infinitely long column of liquid with a spatially harmonic initial disturbance and study its temporal growth. It can be shown that the two approaches are identical for high-velocity jets, i.e. when the average stream speed is much higher than the capillary wave speed. Here, we only consider the temporal instability analysis.

We consider the temporal evolution of a liquid jet inside a vacuum or another immiscible fluid which exerts uniform pressure and negligible drag on the jet. The variables are non-dimensionalized by the radius of the undisturbed jet, r_o, and a characteristic time scale, $(\rho r_o^3/\gamma)^{1/2}$. The governing equations for the problem are

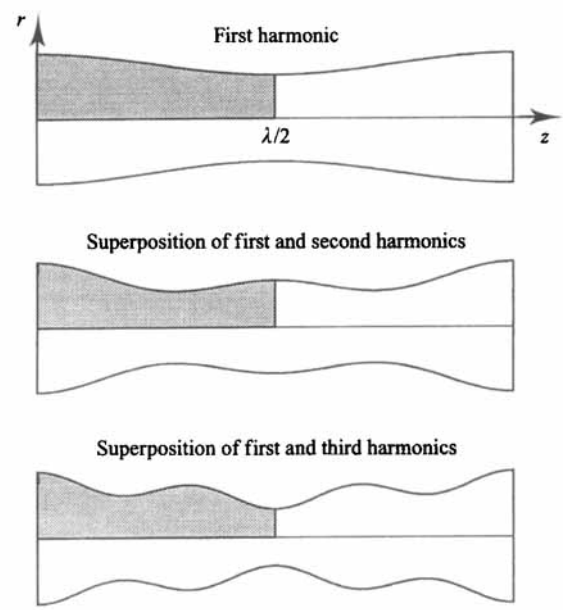

FIGURE 1. Surface disturbances generated by the superposition of the harmonics. The shaded area indicates the computational domain.

those of continuity and the momentum in axisymmetric coordinates (r, z) which in non-dimensional form are written as

$$\nabla \cdot \boldsymbol{u} = 0, \tag{1}$$

$$Re\frac{\mathrm{D}\boldsymbol{u}}{\mathrm{D}t} = \nabla \cdot \boldsymbol{T}, \tag{2}$$

where $\boldsymbol{u} = (u, v)$ is the velocity vector and $\boldsymbol{T} = -p\boldsymbol{I} + [\nabla \boldsymbol{u} + (\nabla \boldsymbol{u})^T]$ is the stress tensor for Newtonian fluid. $\mathrm{D}/\mathrm{D}t$ is the total derivative operator defined as $\mathrm{D}/\mathrm{D}t = \partial/\partial t + \boldsymbol{u} \cdot \nabla$. The gravity effects are neglected. Stress balance on the free surface provides the following boundary condition, assuming the ambient pressure as the datum: $\boldsymbol{T} \cdot \boldsymbol{n} = ReK\boldsymbol{n}$, on the free surface, where $\boldsymbol{n}$ is the outward unit normal and K is the curvature of the surface. Assuming that the surface of the jet can be described by a height function $h(z, t)$, the curvature is given by $K = [h_{zz}/(1 + h_z^2)^{3/2}] - [1/h(1 + h_z^2)^{1/2}]$, where subscript z refers to the derivative with respect to z.

At the centre of the jet the symmetry conditions are applied: $\partial u/\partial r = 0$, and $v = 0$ at $r = 0$. Since a temporal analysis is considered here, the simulations can be restricted to the half of the disturbance wavelength (i.e. the non-dimensional wavelength of the first harmonic, λ) using the symmetry. The shaded area in figure 1 shows the computational domain. The symmetry boundary conditions for the ends of half a wavelength are $u = 0$ and $\partial v/\partial z = 0$ at $z = 0$ and $\lambda/2$.

An imposed surface disturbance as well as a zero velocity field constitute the initial conditions for the jet. The surface disturbance, η, is composed of the superposition of two wavenumbers:

$$\eta(z) = \epsilon_1 \cos(kz) + \epsilon_n \cos(nkz + \theta) \quad \text{at} \quad t = 0, \tag{3}$$

where k and ϵ_1 respectively represent the wavenumber and the amplitude of the first harmonic (also referred to as the fundamental disturbance), ϵ_n represents the

amplitude of the nth harmonic, and θ is the phase angle between the first and the nth harmonic input. The above boundary conditions limit the study to $\theta = 0$ and $\theta = 180°$ only. Here, we have considered the superposition of the first and second harmonics, and the first and third harmonics. The surface of the jet is defined by

$$r = R + \eta(z, t), \tag{4}$$

where R is determined so that the volume of the jet is kept constant when the initial disturbance amplitude is changed:

$$R = \left(1 - \frac{\epsilon_o^2}{2} - \frac{\epsilon_n^2}{2}\right)^{1/2}. \tag{5}$$

By changing the amplitudes of these disturbances, a wide range of initial surface shapes can be produced. Figure 1 shows the typical shapes of the three cases that are considered here.

The method of solution is the height–flux method (HFM) developed by Mashayek & Ashgriz (1993) which was later used to study the capillary (Ashgriz & Mashayek 1995; Mashayek & Ashgriz 1995*b*) and thermocapillary (Mashayek & Ashgriz 1995*a*) instability of liquid jets. This method is based on a Galerkin finite element method with penalty formulation, and a flux method for surface advection. Very briefly, the fluid domain is subdivided into small subvolumes along the jet axis. The subvolumes are then used to find a height function which describes the location of the jet surface. The jet surface in each pair of neighbouring subvolumes is approximated by a line segment and its slope is calculated using the volume of the fluid in the two subvolumes. Then, the volume flux from each subvolume to its neighbouring one is calculated. Thus a new height function and consequently a new surface for the jet is obtained. The accuracy of the method has been tested carefully and typical tables indicating the convergence of the method with the decrease of the mesh size and the time step are given in Ashgriz & Mashayek (1995) and Mashayek & Ashgriz (1995*a*). A similar approach is adopted in the current work to assure the accuracy of the results.

The computational time step is variable during one simulation. Generally, smaller time steps are needed at the beginning of the simulation and near the breakup point. The time steps are decreased until the difference between two successive simulations is less than 2% for the drop sizes and the breakup time. More than 800 simulations have been completed. The computations are stopped and the breakup time is defined when the minimum radius of the jet becomes less than 1% of the undisturbed radius. In each simulation, the volumes obtained for the main drop and the satellite drop at the breakup point are used to compute the radius of the drops produced.

3. Superposition of the first and second harmonics

3.1. *The breakup mechanism*

The theoretical investigations of capillary jet breakup indicate that for small disturbance amplitudes, the cut-off wavenumber is close to $k_c = 1$ (Rayleigh 1879; Chandrasekhar 1961). Disturbances with $k > k_c$ will not grow and will only oscillate. This is important when superposition of two different wavenumbers is used to disturb the jet (*wavenumber* in our temporal analysis is the equivalent of the *frequency* (f) used in spatial analysis for a constant jet velocity (V_{jet}), i.e. $k = 2\pi r_o f / V_{jet}$). For instance, if both wavenumbers are below the cut-off wavenumber, they both will grow; and if one is below and the other is above the cut-off wavenumber, one will grow while the other will oscillate. We have limited our study to a single Re of 200. The satellite drop

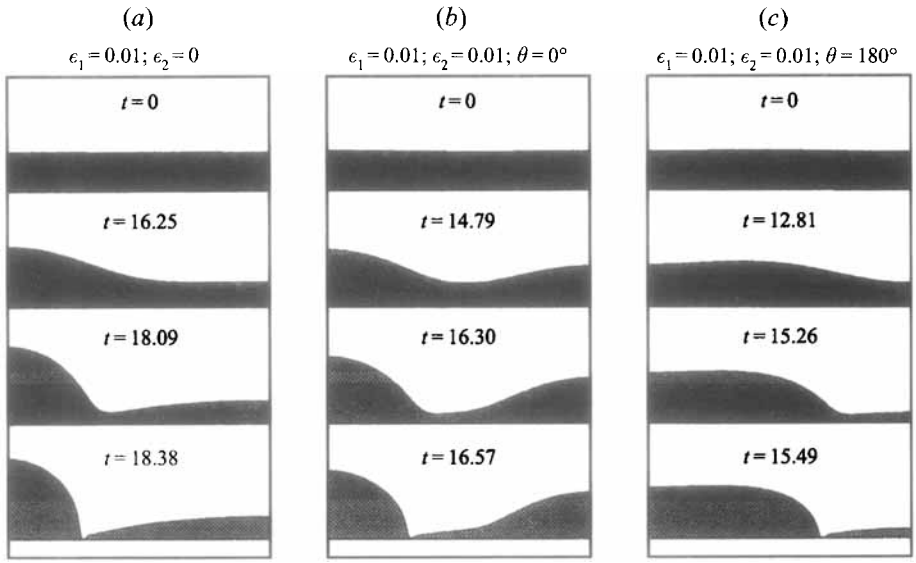

FIGURE 2. Jet breakup by the addition of an unstable second harmonic. $k = 0.45$ and $Re = 200$.

sizes generated from small Reynolds number jets are relatively small, and therefore, those jets are not suitable for satellite size control. Drop sizes can be changed in a much wider range for larger Re.

3.1.1. *Unstable second harmonic*

Here, we discuss the mechanism of the breakup of a liquid jet subject to a disturbance composed of the superposition of the first and second harmonics. For small disturbance amplitudes, if the wavenumber of the first harmonic is less than 0.5 the second harmonic is unstable. On the other hand, if the wavenumber of the first harmonic is greater than 0.5, the second harmonic is stable. Figure 2 presents typical breakup patterns for half of a wavelength (shaded area in figure 1) obtained with an unstable second harmonic. The wavenumber considered is 0.45 and the amplitudes of the first and second harmonics are both 0.01. For these simulations, 70 elements were used in the axial direction and 4 elements in the radial direction. In the following description, the point at $z = 0$ and the point at $z = \lambda/2$ are referred to as the swell and the neck points, respectively (they are respectively the crest and the trough of the first-harmonic surface disturbance). In the case of a single-wavenumber disturbance (figure 2*a*), the jet remains sinusoidal during the larger portion of the breakup time until a cylindrical thread is formed. A contraction then appears at the joint between the bulbous swell region and the ligament thus creating a local pressure maximum which accelerates the detachment of the ligament by pushing the liquid away from that point. With the second harmonic input (figure 2*b*), a contraction is formed around $\lambda/4$. The breakup occurs at one end of the ligament, resulting in a large satellite. When a phase angle of 180° is used, an almost opposite evolution of the jet occurs as shown in figure 2(*c*). Here, a bulging of the central region is observed and two contractions are formed at the swell and the neck points. The contraction at the neck point leads to the formation of a small ligament, which after pinch-off will produce the satellite drop. Notice that the breakup time is reduced when using an unstable second harmonic.

In order to explain the shape evolutions observed in figure 2, the linear modes of the

surface shape and their temporal evolution during the breakup process are determined. A discrete Fourier decomposition is used to analyse the jet radial displacement:

$$r(z,t) = R + \sum_{n=0}^{\infty} \epsilon_n \cos(nkz). \tag{6}$$

The orthogonality of the cosine functions is used to compute the coefficients ϵ_n. Figure 3 shows the temporal evolution of the first, second, third and fourth harmonics associated with figure 2. As expected, the first harmonic is unstable and grows with time. For a monochromatic perturbation (figure 3*a*), the higher harmonics grow rapidly only near the breakup point. The satellite formation is the direct consequence of the growth of these harmonics. With a second-harmonic input, the breakup process is seen to be dominated by the second harmonic which grows much faster than the first (see figure 3*b*). The high positive amplitude of the second harmonic explains the formation of the neck at $\lambda/4$ observed in figure 2(*b*). When using a phase angle of 180°, the initial amplitude of the second harmonic is negative and its growth results in a high negative amplitude as shown in figure 3(*c*), which is favourable for the reduction of the satellite size.

The results of figure 3 can also be explained based on the analytical solution of Chaudhary & Redekopp (1980) who studied the capillary instability of the jet subject to an initial velocity disturbance of the form $\eta(z, t = 0) = 0$ and $\partial\eta/\partial t(z, t = 0) = \epsilon_1\omega_0 \cos(kz) + \epsilon_n\omega_0 \cos(nkz + \theta)$, where ω_0 is a characteristic scaling frequency given by the linear dispersion relations (Rayleigh 1879). They found the following first- and second-order solutions (their third-order solution is not given here):

$$\eta_1 = B_{11} \cos(kz) + B_{12} \cos(nkz + \theta), \tag{7}$$

$$\eta_2 = B_{21} \cos(2kz) + B_{22} \cos[2(nkz+\theta)] + B_{23} \cos[(n-1)kz+\theta] + B_{24} cos[(n+1)kz+\theta] + B_{20}. \tag{8}$$

The coefficients B_{ij} are defined in Chaudhary & Redekopp (1980). The first term, $\cos(2kz)$, of the second-order solution represents the generation of the second harmonic due to the first: this explains the growth of the second harmonic when using a single sinusoidal disturbance as shown in figure 3(*a*). For a second-harmonic input ($n = 2$), the third and fourth harmonics are also generated immediately by the second-order solution ($\cos[(n + 1)kz + \theta]$ and $\cos[2(nkz + \theta)]$). The third term ($\cos[(n-1)kz+\theta]$) represents a feedback from the second harmonic to the first. Hence, a second-harmonic input generates interactions between the first four harmonics only by considering the second-order solution. The results of figures 3(*b*) and 3(*c*) can be explained by noting that the first term $\cos(2kz)$ of the second-order solution does not contain the input phase angle θ. The amplitude of the second harmonic for $n = 2$ based on the first- and second-order solutions is $B_{12} \cos(2kz+\theta) + B_{21} \cos(2kz)$. Therefore, for $\theta = 0$ the two terms add together resulting in a relatively large increase in the amplitude of the second harmonic as shown in figure 3(*b*). However, for $\theta = 180°$ they are subtracted from each other resulting in a relatively small increase in the amplitude of the second harmonic as shown in figure 3(*c*).

3.1.2. *Stable second harmonic*

Next, the breakup of a jet subject to a disturbance consisting of a fundamental and a stable second harmonic is discussed. The computations are performed with $k = 0.7$ with 50 elements in the axial direction and 4 elements in the radial direction. The amplitudes of the first and second harmonics are 0.01 and 0.10, respectively. Here, a

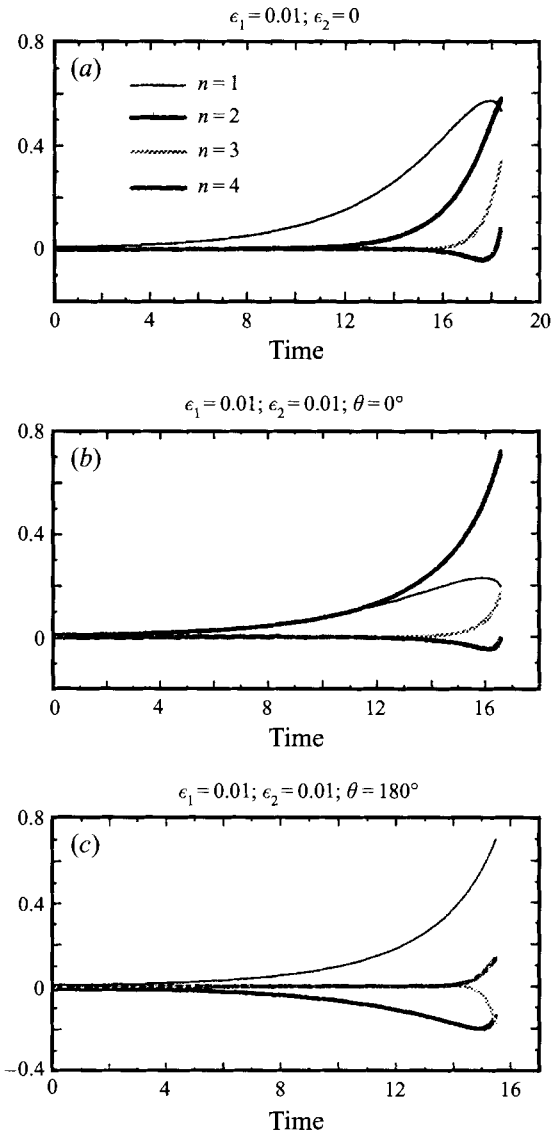

FIGURE 3. Temporal variations of the amplitudes of the harmonics for an added unstable second harmonic. $k = 0.45$ and $Re = 200$.

large initial disturbance amplitude for the second harmonic is presented, since smaller amplitudes do not show a significant change in the breakup of the jet. A more detailed study of the amplitude effect is presented in §3.3.

The addition of a stable second-harmonic component to the initial disturbance results in the oscillation of the jet surface followed by a contraction of the neck point and the growth of the swell point, leading to the formation of a ligament. Two very different breakup configurations are obtained depending on the phase angle, which are explained by considering the temporal evolution of the harmonics shown in figure 4. The first harmonic is the main cause of the jet instability. The second harmonic is stable, as shown by the slightly damping oscillations in figures 4(*b*) and 4(*c*). Because the second harmonic is oscillating, its sign near the breakup point can be

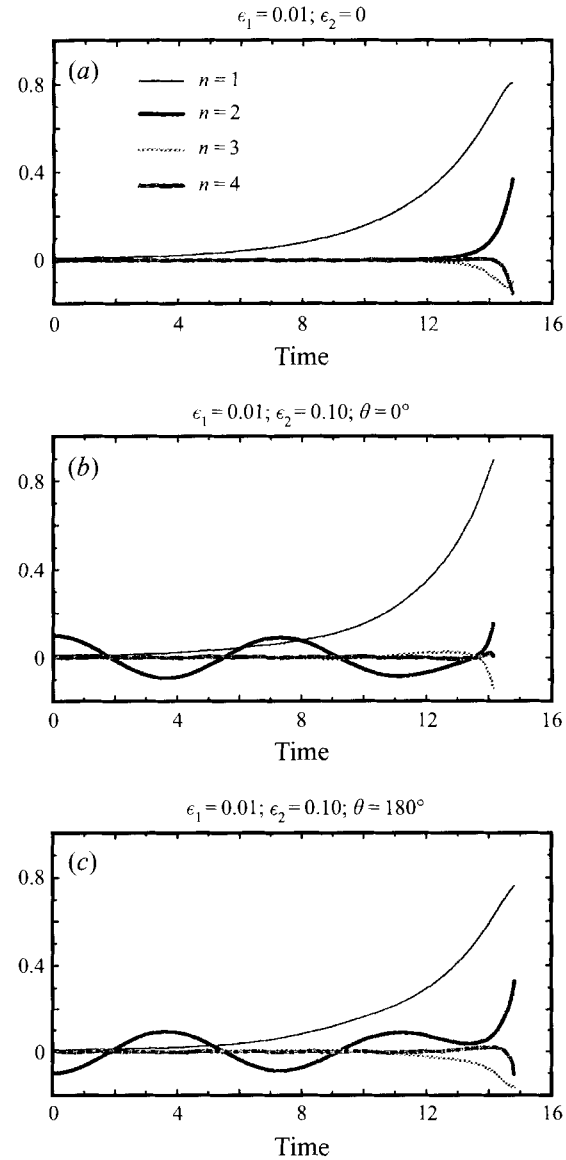

FIGURE 4. Temporal variations of the amplitudes of the harmonics for an added stable second harmonic. $k = 0.7$ and $Re = 200$.

either positive or negative. This has a major influence on the outcome of the breakup (this effect is further discussed in §3.2). Initially, the crest of the second harmonic is at $\lambda/2$ and its trough is at $\lambda/4$ as shown in figure 1. Thus, it is preventing the jet from breaking at $\lambda/2$ and, therefore, contributes to the formation of the satellite. Conversely, a negative amplitude of the second harmonic acts in the same direction as the first harmonic and helps the jet to break at $\lambda/2$.

3.2. *Effect of the wavenumber*

In this section, the breakup of the jet for non-dimensional wavenumbers of the first harmonic ranging from 0.2 to 0.9 are investigated. The initial amplitudes of

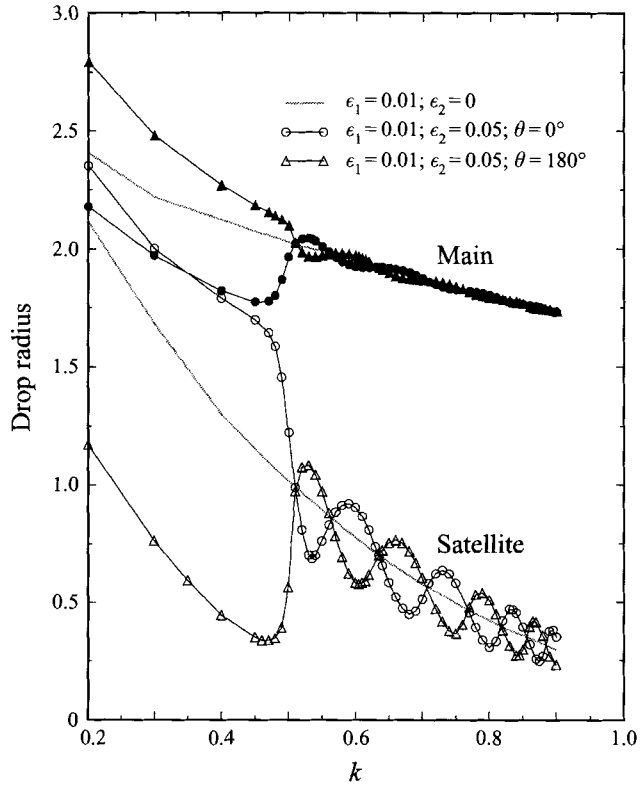

FIGURE 5. Variations of the main and the satellite drop sizes with the wavenumber for $Re = 200$.

the sinusoidal disturbances are kept constant at $\epsilon_1 = 0.01$ and $\epsilon_2 = 0.05$. The initial domain is discretized into 40 to 90 subvolumes depending on the wavenumber considered.

Figure 5 shows the variation of the main and satellite drop sizes versus the wavenumber of the first harmonic. Three sets of results are presented in this figure: (i) first harmonic, only; (ii) added second harmonic with $\theta = 0$; and (iii) added second harmonic with $\theta = 180°$. Two different behaviours are observed. For $k < 0.5$, when the added second harmonic is unstable, the breakup is highly dependent on the initial phase of the second-harmonic input. For no phase difference, the initial positive amplitude of the unstable second harmonic leads to satellites much larger than when no second harmonic is added. For very small wavenumbers, the satellite drop becomes larger than the main drops. For $\theta = 180°$, which is equivalent to an initial negative amplitude of the second harmonic, the satellite drop sizes are significantly reduced.

Two factors are competing here. One is the change in the growth rate with changing wavenumber and the other is the increase in the satellite drop size with the increase in the wavelength (i.e. reducing the wavenumber). For $k > 0.5$, the drop sizes oscillate when a second harmonic, either with or without phase angle, is added. Therefore, in comparison with the monochromatic disturbance, the addition of a second harmonic can result in an increase or a decrease of the satellite size, depending on the wavenumber of the first harmonic disturbance and the value of the initial phase angle. The oscillations have several remarkable characteristics. (i) They are located around the curve obtained with no second harmonic input, and the part

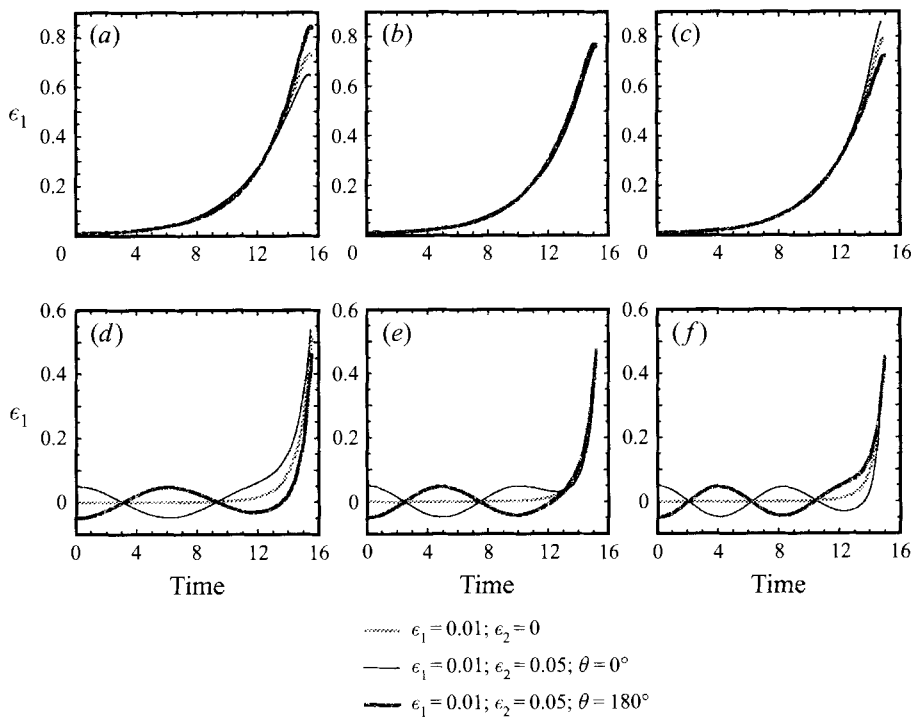

FIGURE 6. Temporal variations of the amplitudes of the first and the second harmonics for $k = 0.60$, 0.635, and 0.67.

of the oscillatory curve located below the dotted line has slightly larger amplitudes than the part above it. (ii) The wavelength of these oscillations is not constant: it first increases then decreases with increasing disturbance wavenumber of the first harmonic (more oscillations are observed for large wavenumbers). (iii) The amplitude of the oscillations is decreasing with increasing wavenumber. (iv) The initial phase of 180° results in a curve which has a wavenumber-dependent phase difference with that obtained with no phase input (the local extrema of the two curves are at slightly different wavenumbers) and their intersection points are located on the curve of the monochromatic disturbance.

This oscillatory behaviour can be explained by considering the evolution of the harmonics. Figure 6 shows the temporal evolution of the first and the second harmonics for three particular values of the wavenumber: $k = 0.635$, which is approximately an intersection point between the three curves (see figure 5), $k = 0.60$, and 0.67, where large differences in the satellite size are obtained when using a phase angle for the second harmonic. Figure 6 reveals that the initial phase input of the second harmonic remains constant for a large portion of the breakup time. The evolution of the first harmonic is similar for all three wavenumbers until the second harmonic becomes unstable. For $k = 0.60$ (figure 6*a*,*d*), the second harmonic becomes unstable just after having reached a maximum (minimum) for $\theta = 0°$ ($\theta = 180°$). After the second harmonic becomes unstable, the first harmonic for $\theta = 180°$ grows much faster than the one for $\theta = 0°$, resulting in a significant amplitude difference at the breakup point. On the other hand, there is only a slight difference in the amplitudes of the second harmonic at the breakup point. Therefore, the large difference observed in the satellite sizes is related to the sign of the second harmonic at the time it becomes unstable.

A similar discussion can be given for $k = 0.67$ (figure 6*c,f*). Here, the second harmonic has three oscillations as opposed to the two oscillations of $k = 0.60$ and the sign of the second harmonic at the time it becomes unstable is the opposite of the previous case. As a result, at the breakup point, the amplitude of the first harmonic for $\theta = 0°$ is higher than that for $\theta = 180°$ while the amplitudes of the second harmonic are almost the same. Hence, there is a significant decrease (increase) of the satellite size for $\theta = 0°$ ($\theta = 180°$). Using a phase angle of $\theta = 180°$, i.e. imposing a negative amplitude of the second harmonic, essentially results in changing the sign of the second harmonic at the time it becomes unstable, since the period of the oscillations remains the same. For $k = 0.635$ (figure 6*b,e*), the amplitudes of the second harmonic for $\theta = 0°$ and $\theta = 180°$ are almost equal and close to zero when the second harmonic becomes unstable. The later evolution of the first and second harmonics is similar for all three cases considered which, consequently, results in identical breakup configurations.

From these observations, the time when the second harmonic becomes unstable, t_s, appears to be a major factor in determining the outcome of the jet breakup. The satellite is smaller (larger) than that produced by a single-wavenumber disturbance when the amplitude of the second harmonic is negative (positive) at $t = t_s$. It can be concluded that the drop size oscillations are caused when the second harmonic becomes unstable, t_s, and by the variation of the oscillation period of the second harmonic with increasing wavenumber. Assuming a linear temporal oscillation of the second harmonic, the amplitude of the second harmonic at t_s is given by

$$(\epsilon_2)_s = \epsilon_{20} \cos(\omega_2 t_s) \tag{9}$$

where ϵ_{20} is the initial amplitude of the second harmonic (*e.g.* $\epsilon_{20} = \pm 0.05$ for $\theta = 0°$ and 180°) and ω_2 is defined by Rayleigh (1879):

$$\omega_n = \left(\frac{\gamma}{\rho r_o^3}\right)^{1/2} \left[\frac{I_1(nk)}{I_o(nk)}\left((nk)^2 - 1\right)nk\right]^{1/2}, \tag{10}$$

for $n = 2$.

Based on the discussion given for figure 6, it can be assumed that the satellite size is minimum when the second harmonic is minimum at t_s and vice versa, i.e. $(\epsilon_2)_s \approx \pm 0.05$ at the wavenumbers associated with the local extrema of the satellite sizes. Therefore, t_s can be determined at these particular wavenumbers. For instance, for $\theta = 0$, $t_s = 2\pi m/\omega_2$ at the wavenumbers corresponding to local maxima of satellite size (i.e. $k = 0.59$, 0.73, 0.835, and 0.895), and $t_s = (2m - 1)\pi/\omega_2$ at the wavenumbers corresponding to local minima of satellite size (i.e. $k = 0.535$, 0.68, 0.80, and 0.875), where m is chosen so that t_s has the highest value below the breakup time. Assuming that the breakup is only due to the growth of the first harmonic the breakup time, $\tilde{t}_b$, is predicted by Rayleigh's theory:

$$\tilde{t}_b = \frac{1}{\omega_1} \ln\left(\frac{1}{\epsilon_{10}}\right) \tag{11}$$

where ϵ_{10} is the initial amplitude of the first harmonic (here $\epsilon_{10} = 0.01$) and ω_1 is the growth rate of the first harmonic, given by equation (10) with $n = 1$. The results of the numerical simulations revealed that $\tilde{t}_b$ was always located between t_s and the actual breakup time and that the difference between $\tilde{t}_b$ and t_s is oscillatory. Assuming $\tilde{t}_b$ to be a good approximation of the time of instability of the second harmonic, equation (11) provides a continuous variation of t_s with increasing wavenumber. The

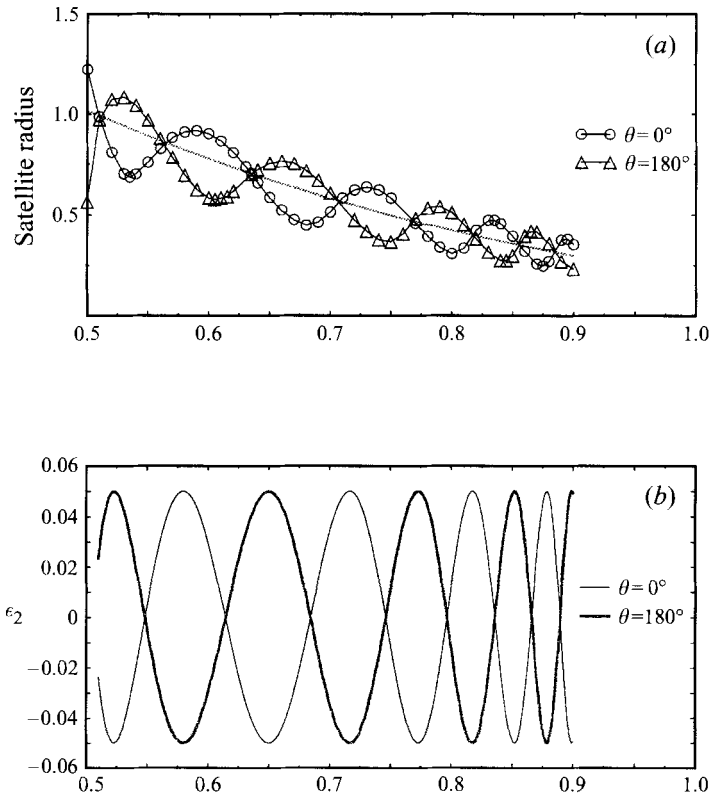

FIGURE 7. Comparison of the oscillations in the satellite drop size (*a*) obtained from the simulations with (*b*) the oscillations predicted for the amplitude of the second harmonic using the linear theory.

amplitude of the second harmonic at t_s can then be determined using equation (9). Figure 7(*b*) shows the variations of $(\epsilon_2)_s$ with increasing wavenumber which are to be compared with the oscillations of the satellite drop size given in figure 7(*a*). The two oscillations are qualitatively similar, however the extrema do not occur at the same wavenumbers. The differences between the oscillations become larger at larger wavenumbers since the error caused by assuming $\tilde{t}_b$ to be the time when the second harmonic becomes unstable is larger relative to the oscillation period of the second harmonic which decreases with increasing the wavenumber.

The variation of the breakup time with the wavenumber, k, is shown in figure 8 for $\epsilon_2 = 0.05$ and $\theta = 0$. Similar evolution of the breakup time is obtained for the two values of phase angle considered. Therefore, we have only plotted the results obtained with the second-harmonic input with no phase angle, along with the case of a monochromatic disturbance. With the monochromatic disturbance, the breakup time reaches a minimum corresponding to the most unstable wavenumber, which is also analytically predicted by Chandrasekhar (1961). When a second harmonic is added, two distinct evolutions are obtained as seen previously for the drop size variation with wavenumber. When the second harmonic is unstable ($k < 0.5$), the breakup time is much smaller than in the case of a monochromatic disturbance and a minimum is achieved close to $k = 0.35$. This is close to the wavenumber of maximum growth rate for the second harmonic according to Rayleigh, i.e. $2k = 0.7$, which shows that the breakup in this region is mainly dominated by this harmonic. A sharp

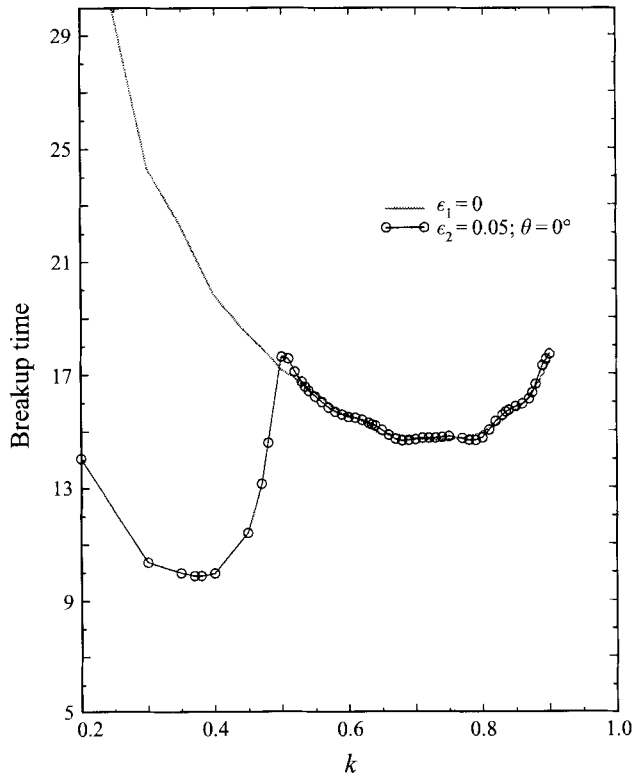

FIGURE 8. Variations of the breakup time with the wavenumber.

increase of the breakup time occurs at the transition to a stable second harmonic. For $k > 0.5$, the second harmonic is stable and the breakup time is very close to that obtained with no second-harmonic input. Small oscillations of the breakup time seem to be occurring around the curve of no second-harmonic input.

3.3. *Effect of the initial amplitude*

3.3.1. *Stable second harmonic*

We first investigate the amplitude effect of a stable second harmonic at $k = 0.7$. For a given input of the first harmonic, the amplitude of the second harmonic is gradually increased until very large initial deformations of the jet surface are obtained. The effects of a phase input is studied by performing the simulations with $\theta = 0°$ and $\theta = 180°$. Figure 9 shows the breakup patterns obtained with a first-harmonic input of $\epsilon_1 = 0.01$. When no phase input is used (figure 9*a*), the increase of the second harmonic gradually reduces the satellite size by moving the breakup location towards the neck. However, a maximum reduction of the satellite is achieved around $\epsilon_2 = 0.15$. The satellite size remains small until $\epsilon_2 = 0.30$ and keeps on increasing thereafter. Meanwhile, the satellite shape is changing from a thin ligament to a bulbous drop for very high inputs of the second harmonic. Figure 9(*b*) shows the breakup patterns obtained for $\theta = 180°$. Results are very different in this case. First, there is an increase of the satellite size until $\epsilon_2 = 0.30$. A cylindrical shape, similar to that obtained with no second-harmonic input is produced at $\epsilon_2 = 0.34$. Then, a slight increase in ϵ_2 results in a sudden relocation of the breakup point, and a significant reduction in the satellite drop size as observed in figure 9(*b*) at $\epsilon_2 = 0.345$. Thereafter, the satellite

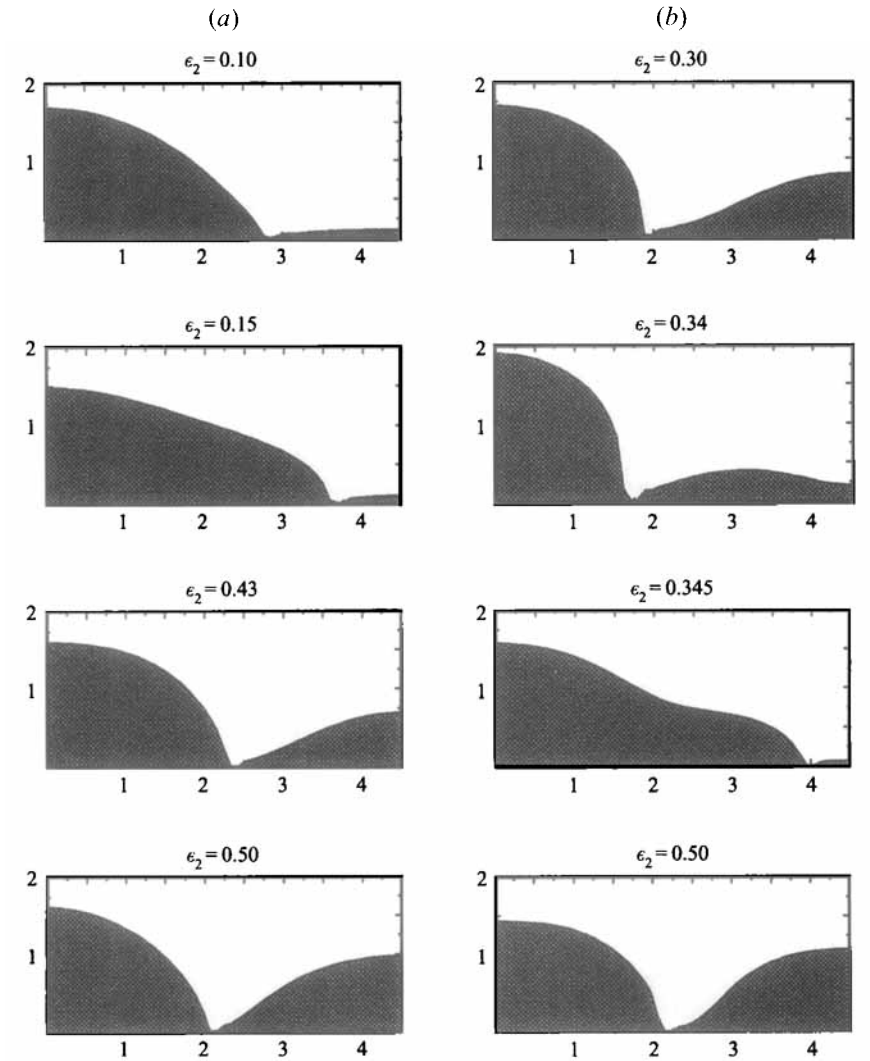

FIGURE 9. Breakup configurations obtained with increasing the initial amplitude of the second harmonic for $k = 0.70$, $Re = 200$, and $\epsilon_1 = 0.01$. (*a*) $\theta = 0°$ and (*b*) $\theta = 180°$.

drop size remains relatively small with increasing ϵ_2 until a second sharp variation is observed at $\epsilon_2 = 0.50$.

As observed previously, it is very helpful to consider the harmonic components of the surface deformation. Figure 10 shows the temporal evolution of the first, second, third and fourth harmonics associated with three amplitudes of figure 9(*a*). It can be seen that the number of oscillations of the second harmonic is constantly decreasing with increasing initial disturbance amplitude. For low inputs of the second harmonic, four extrema can be observed before the breakup, but only two extrema are obtained for very large inputs (i.e. $\epsilon_2 = 0.50$). As discussed earlier, the sign of the second harmonic at the time it becomes unstable is the key factor in the outcome of the jet breakup. Results indicate that no significant change occurs for low inputs of the added harmonic (up to $\epsilon_2 = 0.05$). The second harmonic, after several oscillations, grows near the breakup and reaches a high positive amplitude. For $\epsilon_2 = 0.10$, the

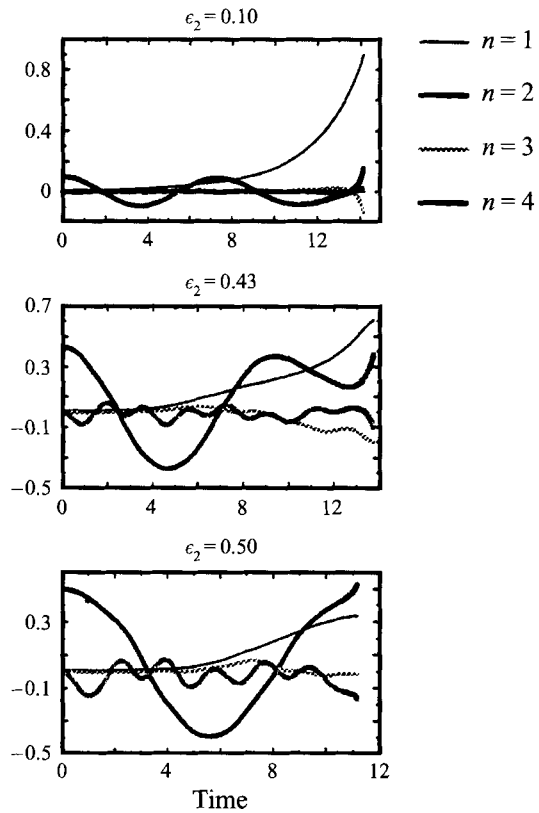

FIGURE 10. Temporal variations of the amplitudes of the harmonics for different values of the initial amplitude of the second harmonic. $k = 0.70$, $Re = 200$, $\epsilon_1 = 0.01$, and $\theta = 0°$.

second harmonic does not grow significantly near the breakup point. This results in a reduction of the satellite size. As the initial input is increased, the oscillations are shortened such that the second harmonic becomes unstable when its amplitude is negative. This change in the sign of the second harmonic is associated with the gradual reduction of the satellite drop. When the initial disturbance amplitude is increased beyond $\epsilon_2 = 0.30$, a reverse phenomenon happens. The amplitude of the second harmonic close to the breakup time is increased, leading to a gradual increase of the satellite size. From $\epsilon_2 = 0.43$ to $\epsilon_2 = 0.50$, the second harmonic becomes unstable at the time its amplitude is positive and, consequently, very large satellites are obtained as shown in figure 9(*a*) at $\epsilon_2 = 0.43$, and 0.50. Similar behaviour is observed for $\theta = 180°$ (see Huynh 1994).

Higher initial amplitudes of the first harmonic are also investigated: ϵ_1 =0.05, 0.1 and 0.2. The drop sizes obtained with increasing the amplitude of the second-harmonic component are presented in figure 11 for $\theta = 180°$. In figure 11(*a,c,d*) the addition of the second harmonic causes the formation of gradually larger satellite drops. Discontinuities are observed in all four curves, at relatively high amplitudes of the second-harmonic input. Here, the discontinuity is referred to the change in the breakup location from one side to the other of the liquid zone. The satellite size is greatly reduced thereafter and remains small with further increase of the second harmonic, except for $\epsilon_1 = 0.01$ where another sharp increase of the satellite size is observed at $\epsilon_2 = 0.50$. The main drop size does not vary significantly except for very

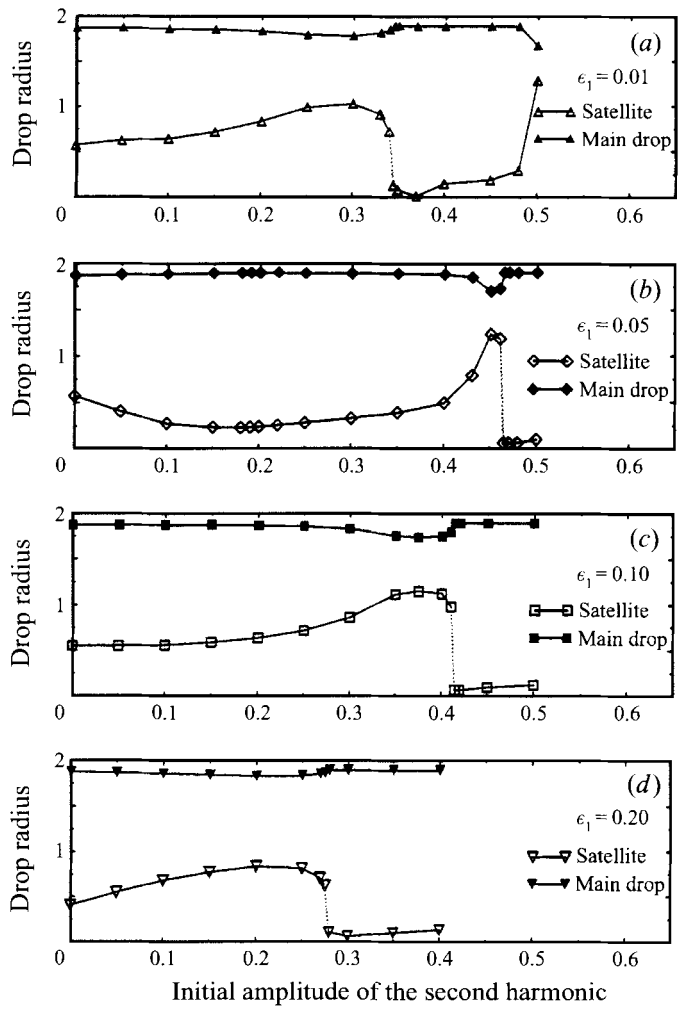

FIGURE 11. Variations of the main and satellite drop sizes with the initial amplitude of the second harmonic for various inputs of the first harmonic. $k = 0.70$, $Re = 200$, and $\theta = 180°$.

high-amplitude disturbances of the second harmonic. At $\epsilon_1 = 0.05$ (figure 11*b*) the change in the satellite size is opposite to the other three cases shown in figure 11(*a*,*c*,*d*). In this case the addition of the second harmonic initially reduces the satellite size. The particular behaviour of the jet breakup shown in figure 11(*b*), is attributed to the initial distribution of the surface energy. (The plots of drop sizes for $\theta = 0°$ are provided in Huynh 1994.)

Figure 12 shows the variations of the breakup time with increasing the initial amplitude of the second harmonic. Large variations in the breakup time are observed around the points where sharp discontinuities in the satellite size are observed. This is due to the fact that the breakup time is closely related to the evolution of the jet radius near the breakup location. Therefore, large variations of the breakup time can result from significant relocation of the breakup point. The breakup time does not vary monotonically with increasing amplitude of the second-harmonic input. As an example, the curve obtained with $\epsilon_1 = 0.01$ and $\theta = 0°$ in figure 12(*a*) shows a gradual decrease of the breakup time until $\epsilon_2 = 0.25$, which corresponds to a gradual

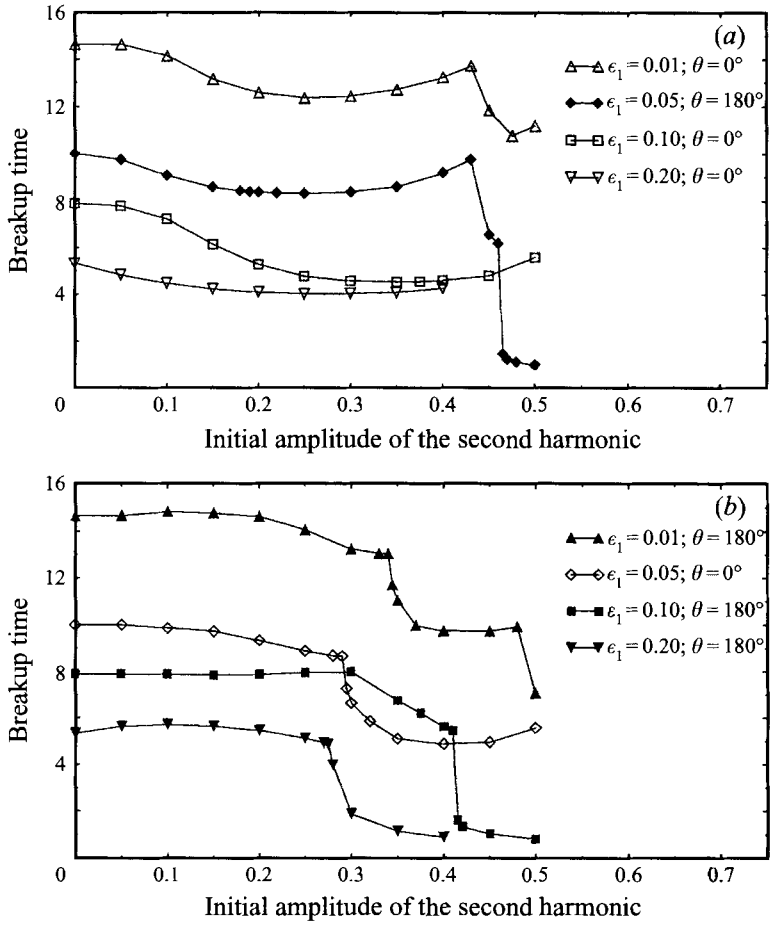

FIGURE 12. Variations of the breakup time with the initial amplitude of the second harmonic for various inputs of the first harmonic. $k = 0.70$ and $Re = 200$.

moving of the breakup location towards the neck point. However, the breakup time then starts to increase again until $\epsilon_2 = 0.43$, which is associated with an increase of the satellite length in figure 9(*a*). The effect of the second harmonic amplitude with $\theta = 180°$ on the breakup time is small for small to moderate amplitudes. A significant decrease of the breakup time occurs for $\epsilon_2 > 0.25$.

3.3.2. *Unstable second harmonic*

We now study the effects of the amplitude of the second harmonic. The wavenumber of the first harmonic considered is $k = 0.45$. As discussed earlier, a positive initial amplitude of the second harmonic usually results in a large satellite size. To reduce the satellite size, we utilized a phase angle of 180° in order to have a negative initial amplitude of the second harmonic. Figure 13 shows the results of simulations performed with increasing initial amplitude of the second harmonic for a constant amplitude of the first harmonic at $\epsilon_1 = 0.01$. For a single-wavenumber disturbance the satellite formation is mainly due to the growth of the second harmonic near the breakup point. As expected, the satellite size is significantly reduced with the first input of the second harmonic, i.e. $\epsilon_2 = 0.005$. However, a small satellite remains even

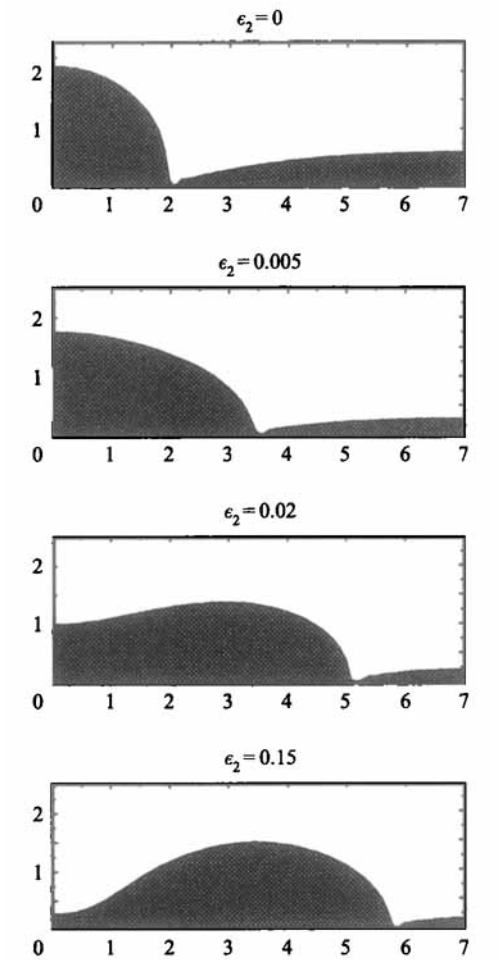

FIGURE 13. Breakup configurations obtained by increasing the initial amplitude of the unstable second harmonic. $k = 0.45$, $Re = 200$, $\epsilon_1 = 0.01$, and $\theta = 180°$.

for very large initial amplitude of the second harmonic. In addition, a contraction is formed at $z = 0$ starting at $\epsilon_2 = 0.02$ and it becomes more pronounced with increasing input of the second harmonic, resulting in the formation of a thin ligament at $\epsilon_2 = 0.15$. This configuration is very unfavourable, since it is likely to lead to further pinch-offs within the main drop. The reason for this is that shifting the second harmonic by 180° results in the formation of two necks: one at $\lambda/2$, which helps to reduce the satellite size, and one at $z = 0$, which is responsible for the formation of the thin thread.

An inspection of the amplitude of the harmonics reveals that since the breakup time is rapidly reduced with increasing inputs of the second harmonic, the first harmonic has less time to evolve and its contribution to the breakup diminishes (see Huynh 1994). Indeed, starting with $\epsilon_2 = 0.15$, the first-harmonic amplitude remains small in comparison with the second-harmonic amplitude. This explains the formation of the slender thread near $z = 0$. The persistence of a small satellite, even though both the first and the second harmonics are contributing to break the jet at $z = \lambda/2$ is due to the generation of higher harmonics through nonlinear interactions.

The variations of the drop sizes with initial ϵ_2 and for different initial amplitude of the first harmonic indicate an immediate reduction of the satellite size for low inputs of the second harmonic. This reduction is faster and more important when the first-harmonic amplitude is small as shown. However, the satellite size does not decrease significantly thereafter and remains almost constant. The ligament length also decreases in the same way with increasing the amplitude of the second harmonic, indicating that the reduction of the satellite size is mainly due to a displacement of the breakup location towards $z = \lambda/2$. In addition, the breakup time rapidly reduces with the first input of the unstable second harmonic. It then continuously decreases with increasing initial amplitude of the second harmonic. The breakup time also decreases with increasing the amplitude of the first harmonic. These results are expected since the increase of either the first or the second harmonics results in an augmentation of the jet instability (see Huynh 1994 for details).

4. Superposition of the first and third harmonics

Figure 14 depicts several breakup configurations for the superposition of the first and third harmonics for $k = 0.45$. With no phase input (figure 14*a*), no significant change is observed for low values of the third-harmonic input. The first remarkable change occurs for $\epsilon_2 = 0.23$. The jet profile shows the formation of a thin ligament connecting two bulbous regions around the swell and the neck points. The slender ligament may break at either of its ends with a small increase of the initial disturbance. A similar pattern occurs at $\epsilon_3 = 0.25$ with a thinner ligament. Similarly to the second-harmonic, sharp changes in breakup configurations are observed for large initial disturbance amplitudes. The large satellite drop produced for $\epsilon_3 = 0.37$ is almost eliminated when increasing the third-harmonic input to 0.38. An even larger variation of satellite size is obtained for higher initial surface deformation.

When a phase angle is added to the third harmonic (i.e. $\theta = 180°$), a slight motion of the breakup point towards the neck along with small modifications of the satellite shape can be observed for low inputs of the third harmonic (figure 14*b*). Significant reduction of the satellite size is achieved when increasing the harmonic input from 0.17 to 0.175, where an almost uniform breakup is obtained. This favourable configuration persists until $\epsilon_3 = 0.37$, after which a second sharp change occurs and results in the formation of a very large satellite at $\epsilon_3 = 0.38$.

An inspection of the temporal evolution of the Fourier coefficients associated with figure 14(*a*) (shown in figure 15) reveals that a necessary condition for the reduction of the satellite size is a positive initial amplitude of the third harmonic. However, this is not sufficient, since the third harmonic is also helping to break the jet around $\lambda/6$. The amplitude of the second harmonic appears to have a significant influence on the size of the satellite drop. Figure 15 shows that the amplitude of the second harmonic at the breakup time is positive up to $\epsilon_3 = 0.37$. At $\epsilon_3 = 0.38$ the amplitude of the second harmonic at the breakup time has become negative, resulting in the formation of a very small satellite drop. The variations of the breakup location observed at $\epsilon_3 = 0.23$ to 0.37 in figure 14(*a*) are attributable to the changes in the amplitude of the third harmonic at the breakup point, resulting from the decrease of the breakup time. When a phase angle of 180° is used, the second-harmonic growth is more quickly reduced. A low amplitude of the harmonic is obtained from $\epsilon_3 = 0.175$ to 0.37, associated with the small satellites of figure 14(*b*). But, the second harmonic amplitude at the breakup is large again for higher inputs of the third harmonic and significant satellites are formed as shown at $\epsilon_3 = 0.38$ of figure 14(*b*).

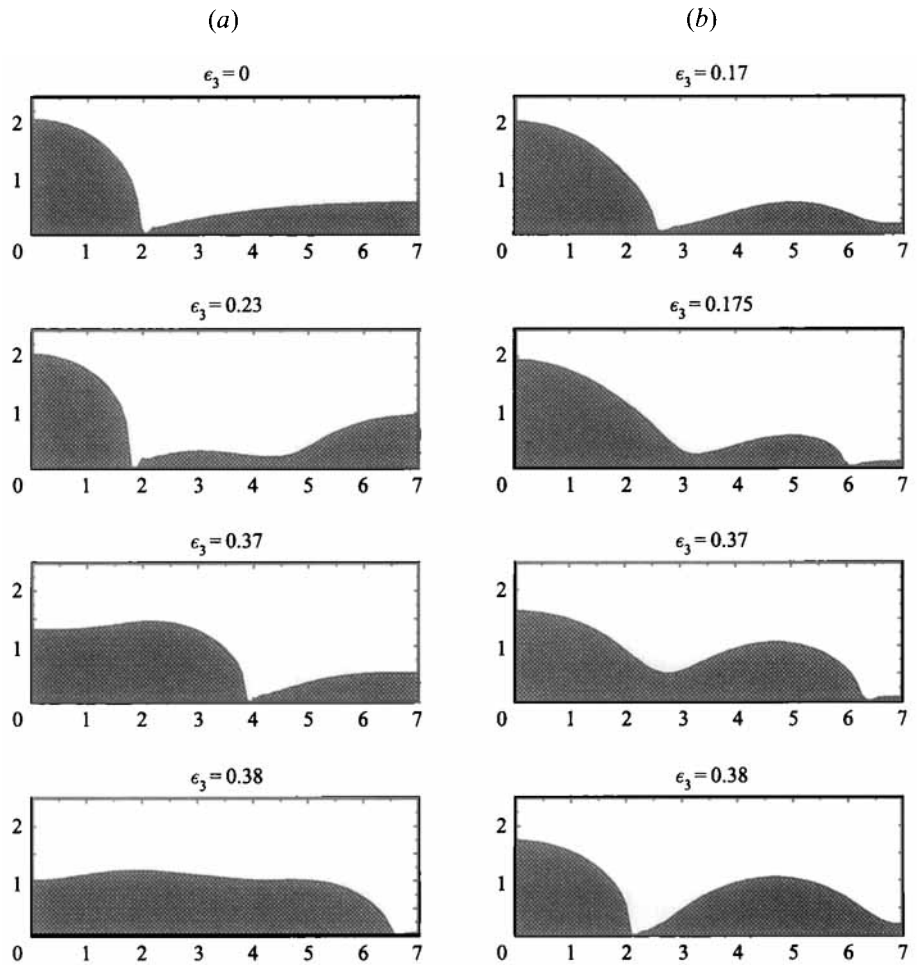

FIGURE 14. Breakup configurations obtained with increasing the initial amplitude of the third harmonic for $k = 0.45$, $Re = 200$, and $\epsilon_1 = 0.01$. (*a*) $\theta = 0°$ and (*b*) $\theta = 180°$.

Figure 15 shows the effects of increasing the third harmonic on the time evolution of the first and second harmonics. It can be seen that the growth of the first harmonic remains the same for the major portion of the breakup time (until around $t = 9.5$) and for a relatively large initial amplitude of the third harmonic ($\epsilon_3 = 0.23$). On the other hand, the second harmonic varies more significantly - with increasing third harmonic input. Large differences between the curves are observed starting at $t = 5$. This is in qualitative agreement with the fact that the interaction of the third and second harmonic is stronger than the feedback from the third to the first as deduced from the analytical results.

Our results can be compared with the nonlinear solution given by Chaudhary & Redekopp (1980). For a third-harmonic input, the second-order solution, (equation 7), shows the formation of the fourth harmonic ($\cos[(n+1)kz+\theta]$) and a second-harmonic ($\cos[(n-1)kz+\theta]$). Interestingly, the feedback to the first harmonic is not present in the second-order solution. In the second-order solution of Chaudhary & Redekopp, equation (7), the term expressing the interaction between the second and the third

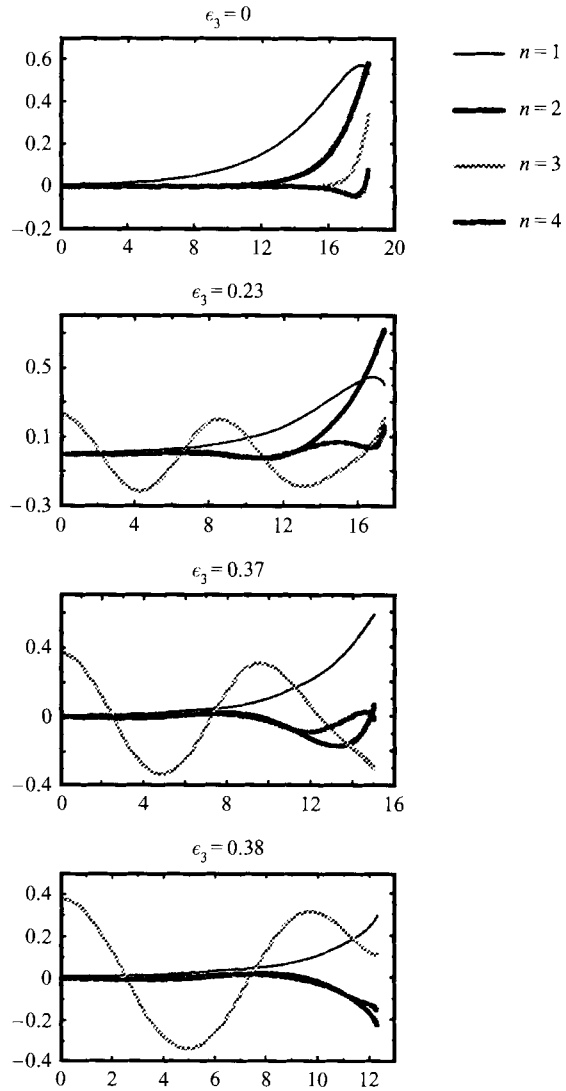

FIGURE 15. Temporal variations of the amplitudes of the harmonics for different values of the initial amplitude of the third harmonic. $k = 0.45$, $Re = 200$, $\epsilon_1 = 0.01$, and $\theta = 0°$.

harmonic is B_{23}. For $n = 3$, this term becomes

$$B_{23} = b_{230}\cosh(\omega_2\tau) + b_{231}\frac{\sinh(\omega_1\tau)}{\omega_1}\frac{\sinh(\omega_3\tau)}{\omega_3} + b_{232}\cosh(\omega_1\tau)\cosh(\omega_3\tau) \qquad (12)$$

where the coefficients b_{ijk} are defined in Chaudhary & Redekopp and ω_n is defined by equation (10).

Since our simulations are performed with $k = 0.45$, ω_1 and ω_2 are real positive while ω_3 is imaginary. Therefore, in B_{23}, the two last terms are products of hyperbolic functions ($\sinh(\omega_1\tau), \cosh(\omega_1, \tau)$) with sinusoidal functions ($\sinh(\omega_3\tau), \cosh(\omega_3, \tau)$), thus resulting in oscillations with increasing amplitudes. Similar temporal evolution of the second harmonic was obtained in our computations as shown in figure 15. This

comparison can only be qualitative as the nature of the initial disturbances in the two cases is different.

Three initial amplitudes of the first harmonic have been investigated: $\epsilon_1 = 0.01$, 0.05 and 0.10. The main and satellite drop sizes obtained with increasing third-harmonic input are shown in figures 16 and 17. In figures 16(*a*) and 16(*c*), no significant reduction of the satellite size is observed for small to moderate initial amplitudes of the third harmonics. However, a sharp discontinuity in size occurs at a larger amplitude. At first, the increase of the third-harmonic input results in a gradual increase of the satellite size. A small reduction is then observed in both curves at $\epsilon_3 = 0.235$ and 0.25 for $\epsilon_1 = 0.01$ and 0.10, respectively. After the discontinuity, the satellite drop sizes become very small. When the amplitude of the first harmonic is increased to $\epsilon_1 = 0.05$, the breakup behaviour significantly changes (figure 16*b*). Here small increases in the amplitude of the added third harmonic decrease the satellite size, followed by a sharp discontinuity at $\epsilon_3 = 0.05$ which further decreases the satellite drop size. At large amplitudes of the third harmonic two discontinuities are observed. The first one increases the satellite size and the second one decreases it. For very large initial amplitudes of the first and third harmonics the breakup time is greatly reduced, therefore the surface has no time to evolve further. For instance, for $\epsilon_1 = 0.10$ (figure 16*c*), the satellite drop size does not increase significantly by changing ϵ_3. For $\theta = 180°$ (figure 17*a*,*c*), however, the addition of the third harmonic initially decreases the satellite drop size slightly. This slight decrease is followed by a sharp discontinuity at higher values of ϵ_3. Its occurrence varies for each amplitude of the first harmonic. A second discontinuity is obtained at high amplitudes of the third harmonic, resulting in the formation of a very large satellite. Note that the sets of results for $\theta = 180°$ differ from those for $\theta = 0$ for very high disturbance amplitude: the satellite remains very large in figures 17(*a*) and 17(*c*), while it is almost eliminated in figure 16(*b*) for $\epsilon_3 > 0.45$. Similar to figure 16, here too the breakup behaviour is different for $\epsilon_1 = 0.05$ (figure 17*b*). The breakup behaviour resembles that of figure 16(*a*) and 16(*c*): the satellite size first increases slightly, shows a small dip at $\epsilon_3 = 0.10$, and then shows two discontinuities. The difference here is that the satellite size remains large at high ϵ_3.

5. Concluding remarks

This paper presents a numerical investigation of capillary jet breakup when the jet is subject to an initial surface disturbance composed of the superposition of a fundamental disturbance (first harmonic) with either its second or third harmonics. Effects of the large-amplitude two-wavenumber disturbances on the drop sizes and the breakup times are investigated. It is observed that such disturbances may result in a variety of breakup configurations, drop sizes and drop shapes. The numerical simulations are completed for a jet with $Re = 200$.

Drop sizes after the breakup depend on whether the added harmonic is stable or unstable. When the added second harmonic is unstable (the wavenumber of the fundamental disturbance is $k < 0.5$), the satellite droplets can be significantly larger or smaller than those formed by a monochromatic disturbance depending on the phase angle between the added harmonic and the fundamental disturbance. With monochromatic disturbances, the satellite formation is mainly related to the growth of the second harmonic near the breakup point. Therefore, adding a second-harmonic disturbance with a negative initial amplitude reduces the satellite drop size and, conversely, a positive initial amplitude increases its size. In the present study a

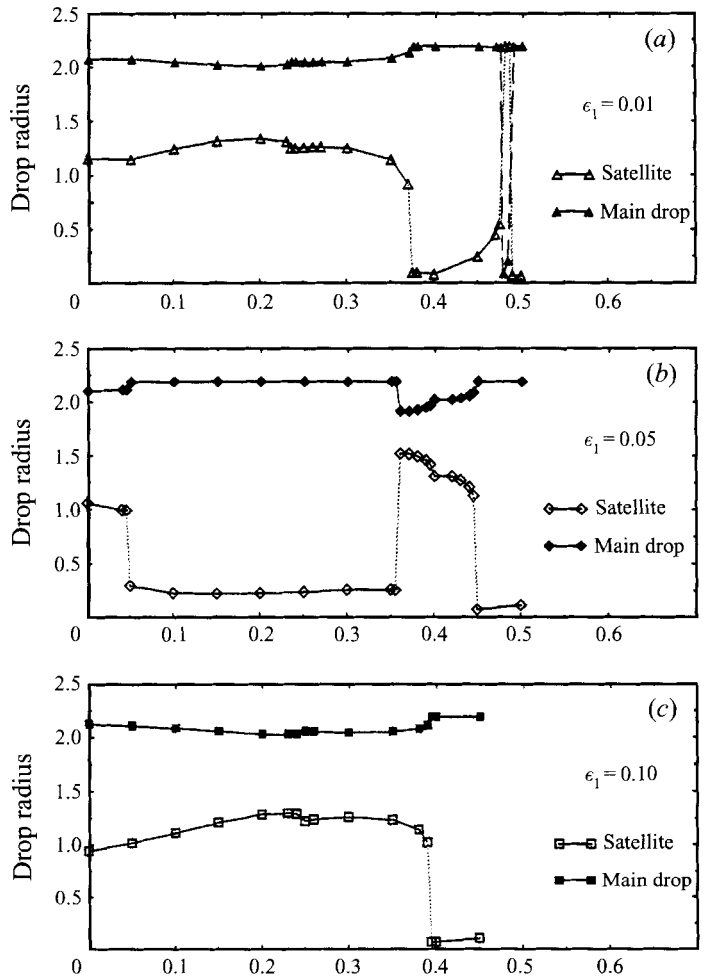

FIGURE 16. Variations of the main and satellite drop sizes with the initial amplitude of the third harmonic for various inputs of the first harmonic. $k = 0.45$, $Re = 200$, and $\theta = 0°$.

negative initial amplitude of the second harmonic is obtained by adding a phase angle of 180° to it.

When the added harmonic, either second or third, is stable, its influence on the droplet size is small for small to moderate amplitudes. An inspection of the temporal evolution of the Fourier coefficients reveals that a favourable condition for the reduction of the satellite size is the addition of a second harmonic with a negative initial amplitude or a third harmonic with a positive initial amplitude. By increasing the amplitude of the added harmonic, the satellite droplet size decreases sharply at a critical amplitude. This critical amplitude depends on the amplitude of the fundamental disturbance and its phase angle with respect to the added harmonic. For a stable added second harmonic and for a constant initial amplitude ratio of the fundamental and its harmonic (ϵ_2/ϵ_1), drop sizes oscillate with increasing the wavenumber of the fundamental disturbance. When the second harmonic is unstable ($k < 0.5$), the breakup time is much smaller than that in the case of a monochromatic disturbance and a minimum is achieved close to $k = 0.35$. A sharp increase of the breakup time occurs at the transition to a stable second harmonic. For $k > 0.5$,

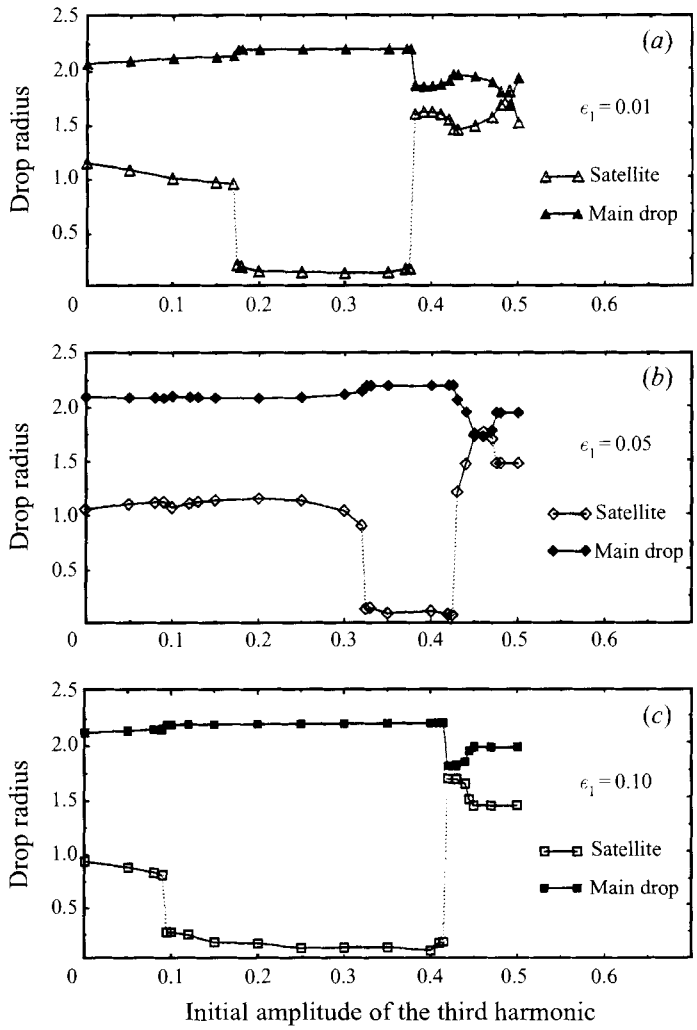

FIGURE 17. Variations of the main and satellite drop sizes with the initial amplitude of the third harmonic for various inputs of the first harmonic. $k = 0.45$, $Re = 200$, and $\theta = 180°$.

the second harmonic is stable and the breakup time is very close to that obtained with no second harmonic input. The breakup time oscillates around that of the monochromatic disturbance on increasing the wavenumber. The amplitude of these oscillations is very small.

The present study clearly shows that a variety of sizes can be generated due to the nonlinear interaction between the two disturbance wavenumbers. This can be useful in ink jet printers where the printing resolution depends on the diameter of the ink drops and, therefore, on the orifice diameter. Using modulated disturbances one can change the printing resolution without changing the orifice diameter.

Finally, a note on the size of the drops formed by the natural breakup of a liquid jet may be timely. Rayleigh (1879) suggested that the fastest growing wavelength is responsible for the natural breakup of a liquid jet, and therefore, the mean size of the drops formed in this process can be determined by this wavelength. However, the superposition of the other disturbances on the fastest growing disturbance and

their relative amplitudes can significantly change the breakup times and the sizes of the drops formed after the breakup. Therefore, a statistical investigation of the sizes formed by the superposition of random disturbances may provide a better estimation of the mean drop size resulting from the natural instability of liquid jets.

REFERENCES

ASHGRIZ, N. & MASHAYEK, F. 1995 Temporal analysis of capillary jet breakup. *J. Fluid Mech.* **291**, 163–190.

BOUSFIELD, D. W., KEUNINGS, R., MARRUCCI, G. & DENN, M. M. 1986 Nonlinear analysis of the surface tension driven breakup of viscoelastic filaments. *J. Non-Newtonian Fluid Mech.* **21**, 79.

BOUSFIELD, D. W., STOCKEL, I. H. & NANIVADEKAR, C. K. 1990 The breakup of viscous jets with large velocity modulations. *J. Fluid Mech.* **218**, 601–617.

CHANDRASEKHAR, S. 1961 *Hydrodynamic and Hydromagnetic Stability.* Claredon.

CHAUDHARY, K. C. & MAXWORTHY, T. 1980*a* The nonlinear capillary instability of a liquid jet. Part 2. Experiments on jet behavior before droplet formation. *J. Fluid Mech.* **96**, 275–286.

CHAUDHARY, K. C. & MAXWORTHY, T. 1980*b* The nonlinear capillary instability of a liquid jet. Part 3. Experiments on satellite drop formation and control. *J. Fluid Mech.* **96**, 287–297.

CHAUDHARY, K. C. & REDEKOPP, L. G. 1980 The nonlinear capillary instability of a liquid jet. Part 1. Theory. *J. Fluid Mech.* **96**, 257–274.

DRESSLER, J. L. 1993 Two-Dimensional, high flow, precisely controlled monodisperse drop source. Rep. WL-TR-93-2049. Wright-Patterson AFB, OH 45433.

HUYNH, H. 1994 Breakup of a capillary jet by frequency synthesis. Master of Science Thesis, State University of New York at Buffalo.

MASHAYEK, F. & ASHGRIZ, N. 1993 A height-flux method for simulating free surface flows and interfaces. *Intl J. Numer. Meth. Fluids* **17**, 1035–1054.

MASHAYEK, F. & ASHGRIZ, N. 1995*a* Nonlinear instability of liquid jets with thermocapillarity *J. Fluid Mech.* **283**, 97–123.

MASHAYEK, F. & ASHGRIZ, N. 1995*b* Instability of liquid coatings on cylindrical surfaces. *Phys. Fluids* **7**, 2143–2153.

ORME, M. & MUNTZ, E. P. 1990 The manipulation of capillary stream breakup using amplitude modulated disturbances: A pictorial and quantitative representation. *Phys. Fluids* A **2**, 1124–1140.

ORME, M., WILLIS, K. & NGUYEN, T.-V. 1993 Droplet patterns from capillary stream breakup. *Phys. Fluids* A **5**, 80–90.

PIMBLEY, W. T. & LEE, H. C. 1977 Satellite droplet formation in a liquid jet. *IBM J. Res. Dev.* **21**, 21–30.

RAYLEIGH, LORD 1879 On the instability of jets. *Proc. Lond. Math. Soc.* **10**, 4–13.

SCHELLER, B. L. & BOUSFIELD, D. W. 1991 Viscous jet breakup: nonsinusoidal disturbances. *Chem. Engng Commun.* **107**, 25–53.

VASSALLO, P. & ASHGRIZ, N. 1991 Satellite formation and merging in liquid jet breakup. *Proc. R. Soc. Lond.* A **433**, 269–286.

YAMADA, T. 1978 Ink-jet recording device with alternate small and large drops. US Patent No. 4,068,241.